Extraction of Power Line Maps from Millimeter-Wave Polarimetric SAR Images

Kamal Sarabandi, *Fellow, IEEE,* and Moonsoo Park

***Abstract*—Radar backscatter of power lines has lower values than those of the surrounding ground clutter when the power line is oriented at an off-normal direction with respect to the radar line of sight. For power lines, the traditional detection algorithms that are commonly based on the statistics of the backscatter power of the clutter and target result in excessive false-alarm rates due to very low signal-to-clutter ratio. In this paper, the application of a statistical polarimetric detection algorithm that significantly improves the signal-to-clutter ratio is demonstrated. The coherence between the co- and cross-polarized backscatter components is used as the detection parameter. This statistical detection parameter can be applied to any extended targets such as a suspended cable in clutter background. Detection criteria based on clutter backscattering coefficients, power line size, and aspect angle, as well as the number of independent samples are obtained. The performance of the algorithm for mapping power lines in SAR images is demonstrated using a number of low-grazing incidence polarimetric SAR images at 35 GHz.**

***Index Terms*—Coherence, detection, polarimetry, power line, synthetic aperture radar (SAR).**

I. Introduction

THE USE of helicopters for military and civilian applications is ever increasing. The civilian applications cover a broad range, which include rescue operations, air ambulance, recreation, construction, etc. Helicopters also have a broad range of applications in the military. They provide superiority over rugged battle fields and constitute a formidable force against armored vehicles and heavy artillery. Operation of these fast low-flying machines, however, is highly limited under poor visibility. The major safety problem is the collision with manmade and natural obstacles such as towers, power lines, and mountains. Due to the existing poor safety records of helicopters, strict safety regulations have been put in place to ensure helicopters stay grounded under conditions of bad visibility even in emergencies. A reliable and all-weather collision warning system rectifies this deficiency. Because of their compact size and all-weather operation capability, millimeter-wave radar systems have been proposed for this purpose [1]. However, detection of hazardous targets in the radar scene is a complicated task and is the subject of many on-going investigations.

Manuscript received September 20, 1999; revised May 5, 2000. This work was supported by the U.S. Army Research Laboratory under Cooperative Agreement DAAL01-96-2-0001.

The authors are with the Radiation Laboratory, Department of Electrical Engineering and Computer Science, The University of Michigan, Ann Arbor, MI 48109 USA (e-mail: saraband@eecs.umich.edu).

Publisher Item Identifier S 0018-926X(00)07719-X.

A hazardous target of particular interest is an overhead high-voltage power line. A typical scenario of a helicopter approaching a power line in a strong clutter background is depicted in Fig. 1. In the past, several approaches for detecting nearby power line cables have been proposed which include optical and infrared sensors [2], [3]. The detection of power lines, independent of frequency of the sensor, is very challenging since the cross section of these cables are rather small. In many practical situations where there is a significant clutter background, the power line signal-to-clutter ratio is very low. The polarimetric backscatter behaviors of power-line cable have recently been modeled where it is shown that at millimeter-wave frequencies significant backscatter exists only at normal incidence and along certain directions known as Bragg backscatter directions [4]. The spacing between Bragg backscatter directions depends on the cable dimensions (surface period) and the radar wavelength. Nevertheless, it is shown that none of the Bragg modes contribute significantly at incidence angles beyond 15°. The level of backscatter drops significantly at higher angles which is why the detection of power lines using conventional radars is not possible. Experimental results at Ka- and W-band also show the trends predicted by the model [5], [6].

The problem of power-line detection with poor signal-to-clutter was first considered in [5] where a polarimetric detection algorithm was proposed. The performance of this algorithm was demonstrated under laboratory conditions and the results were reported in [6]. In this paper, the performance of the algorithm is further examined using polarimetric SAR images at 35 GHz. The motivation behind this investigation is twofold: 1) to examine the accuracy of the polarimetric algorithm using real data, and 2) to demonstrate the feasibility of mapping power-line networks using remote sensing data. While the location of power lines are well documented in friendly areas, knowledge of their exact location in unfriendly regions is often inaccurate and, in some cases, not available. In what follows, a brief description of the polarimetric detection algorithm is given. Then the general behavior of polarimetric response of clutter at millimeter-wave frequencies is considered. In Section IV an analytical approach for performance evaluation of the algorithm is presented. In this section the relationship between the required number of independent samples for a given false alarm rate in terms of radar aspect angle and power line backscatter level is developed. In Section V, the performance of detection algorithm in detecting power lines in 35-GHz radar images is presented.

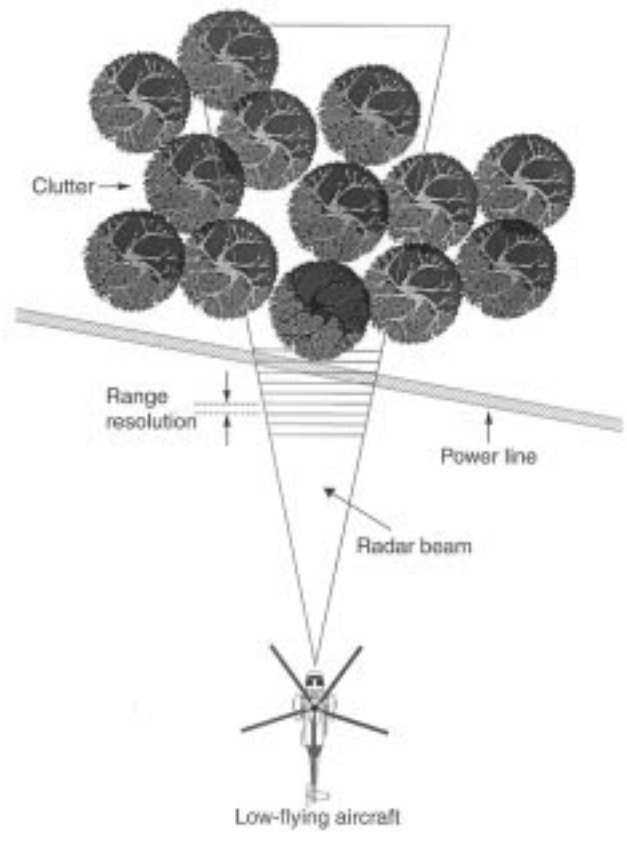

Fig. 1. A scenario of a helicopter approaching a power line in a strong clutter background.

II. Detection Algorithm

In this section, the basic concept of the polarimetric detection algorithm is reviewed. As mentioned earlier, the detection of power lines, either in radar images or when a real aperture radar is used, is hampered by poor signal-to-clutter ratio. In traditional detection algorithms, detection is made by simply comparing the measured radar backscatter to a detection threshold. Hence, for detection, the magnitude of power-line backscatter should be larger than the threshold value, which is usually higher than the mean value of the clutter backscatter coefficient. However, this condition is not met when the aspect angle of the power line is away from near-normal incidence direction. In this situation, there exists no strong backscatter from the power line and the signal-to-clutter ratio is very low. In practice, the backscatter from background vegetation or rough surfaces within the same range as the power line may drastically exceed the backscatter from the power line. This is why conventional nonpolarimetric millimeter-wave radars cannot be used for power-line detection. To circumvent this difficulty, we resorted to radar polarimetry and proposed a statistical detection algorithm to improve the signal-to-clutter ratio.

Theoretical and experimental investigations have shown that the co- and cross-polarized components of backscatter of distributed targets with azimuthal symmetry are statistically uncorrelated [7]. In other words $\langle S_{vv}S_{hv}^{*}\rangle$ and $\langle S_{hh}S_{hv}^{*}\rangle$ vanish for almost all distributed targets provided that the footprint is much larger than the field correlation length in the random medium. However, as was shown in [6] the co- and cross-polarized component of backscatter from power lines are highly correlated ($\langle S_{vv}S_{hv}^{*}\rangle \neq 0$). Measuring $\langle S_{vv}S_{hv}^{*}\rangle$, instead of $\langle |S_{vv}S_{vv}^{*}|^2\rangle$ for example, should improve detection probability drastically.

To circumvent the difficulties associated with radiometric calibration, normalized cross correlation, or namely coherence γ between two radar backscattering components, S_{hv} and S_{vv}, can be used. The coherence between VV and HV channel is defined by

$$\gamma = \frac{\langle S_{vv}S_{hv}^{*}\rangle}{\sqrt{\langle |S_{vv}|^2\rangle\langle |S_{hv}|^2\rangle}}. \tag{1}$$

Assuming that the process is ergodic, the estimate of the coherence can be obtained by substituting the ensemble averages in the above expression with spatial averages. The coherence is estimated from linear section of the image along which a power-line section may exist. A threshold-detection level is then chosen for the coherence estimate, which depends on the required false-alarm rate and probability of detection. The choice of S_{vv} instead of S_{hh} stems from the fact that the backscatter from power lines (away from normal incidence) for VV polarization is higher than that of HH polarization [6]. However, in situations where fully polarimetric data is available, both coherence values can be used for detection of power lines. The probability of detection is a function of number of independent samples, the values of the backscattering coefficient, and the backscatter level of the power line itself. This subject is discussed in detail in Section IV.

III. Backscatter Behavior of Clutter and Power Lines at Millimeter-Wave Frequencies

As mentioned earlier, the probability of detection and the false-alarm rate of power lines depend on the backscatter level of clutter background and its statistics. Over the past two decades, a significant amount of effort has been devoted toward characterizing the backscatter behavior of radar clutter at millimeter-wave frequencies. These activities in general can be categorized into two groups: 1) experimental characterization of clutter backscatter behavior, and 2) theoretical modeling of clutter backscatter. A comprehensive overview of these activities is beyond the scope of this paper, however, a brief discussion related to the problem at hand is provided here. The spectral, angular, and polarimetric behavior of clutter backscatter depends on the clutter type and its physical parameters. Apart from the urban areas, radar clutter may be categorized into three general groups: 1) surfaces, 2) short vegetation and shrubs, and 3) tall vegetation. Backscatter from surfaces at millimeter-wave frequencies is composed of surface scattering and volume scattering [8]–[10]. Surfaces, such as bare soil surfaces, asphalt, gravel, concrete, etc., are heterogeneous media composed of particles of different permittivity whose dimensions are comparable to the wavelength at millimeter-wave frequencies. Depending on the surface roughness and extinction in the medium the surface scattering or volume scattering may be dominant. The backscatter level decreases with increasing the incidence angle and decreasing the frequency. Wet surfaces demonstrate markedly lower backscatter level and low cross-polarized to co-polarized backscatter ratio. The backscatter of surfaces covered with snow is dominated by the volume scattering from the snow [9]–[11]. The level of backscatter of a snow pack decreases with the

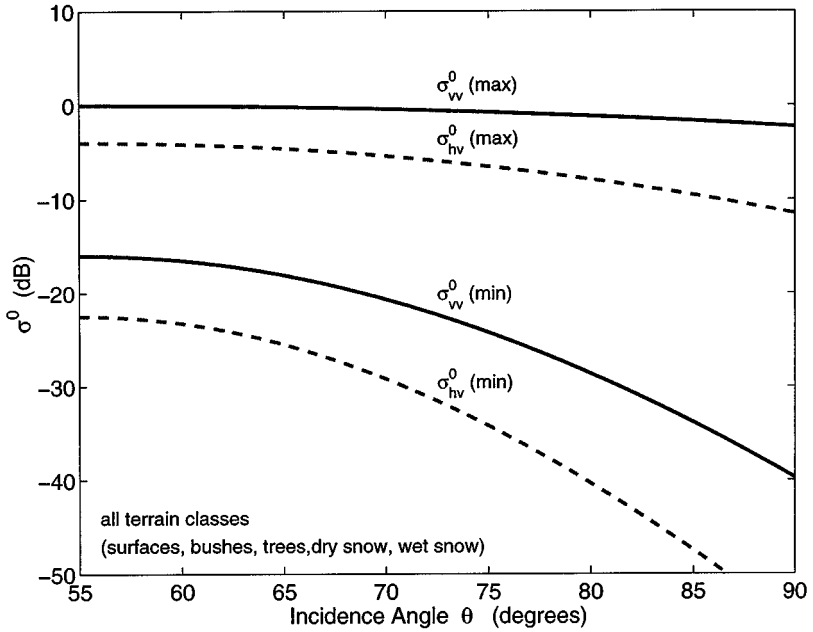

Fig. 2. Dynamic range of σ^0 for terrain at 94 GHz. The maximum and minimum curves represent the upper and lower bound among all measured values reported in [10] and [13].

snow wetness and is a relatively strong function of frequency. Metamorphic snow, which possesses larger ice particles, exhibit higher backscatter. Copolarized backscattering coefficient as high as $+1$ dB for dry snow and -1 dB for wet snow and cross- to co-polarized ratio of -5 dB has been reported in [11].

Due to high-extinction rates in vegetation, backscatter from most vegetation media emanates from the particles near the interface between the canopy and air. The dependence of backscatter to frequency, at millimeter-wave frequencies, is very weak. Usually the level of backscattering coefficients for VV and HH polarizations is similar. Vegetation media also produce significant cross-polarized component, only 4–5 dB below the co-polarized components. Experimental results have shown that for incidence angles higher than 30°, the co-polarized backscattering coefficients at W-band hardly exceed 0 dB and this upper value is reduced for near grazing incidence to about -5 dB. The lower bound, which is produced by impenetrable surfaces with relatively smooth surface roughness, exhibit backscatter levels around -15 dB and have a much faster rate of decrease with incidence angle. For these surfaces, the ratio of cross-polarized to co-polarized backscattering coefficients can be anywhere between -10 dB to -15 dB. Fig. 2 shows the upper and lower bound of σ°_{vv} and σ°_{hv} obtained from measurements of different clutter types at 94 GHz [13].

Radar backscatter behavior of power lines have also been studied extensively over the past few years [4]–[6]. As mentioned earlier, the backscatter up to 15° off normal incidence is dominated by strong Bragg scattering. Away from normal incidence, the backscatter is dropped significantly. However, due to surface irregularity (deviations from perfect periodicity) there are measurable backscatter power at angles beyond 15° incidence. Fig. 3 shows the polarimetric backscatter of a power line with diameter 3.52 cm at 94 GHz [6]. The power line was illuminated by an antenna having a footprint of about 30 cm on the cable. It is observed that σ_{vv} is much higher than σ_{hv} and furthermore considerable cross-polarized backscatter is produced. This is the main reason for choosing the coherence between VV and hv component of backscatter as the detection parameter.

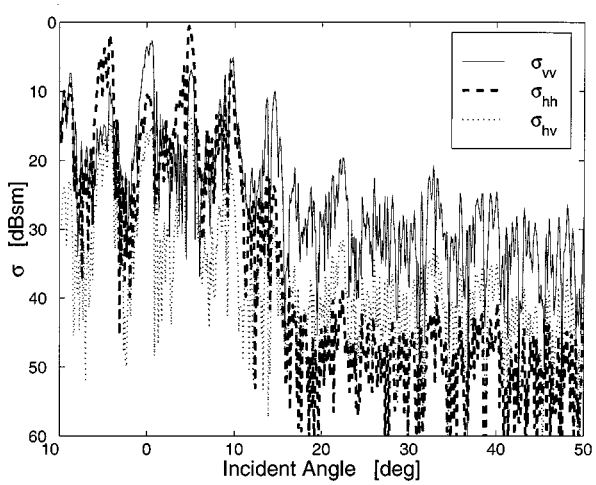

Fig. 3. Angular RCS response of a power line at 94 GHz.

IV. Coherence Estimation

The proposed detection algorithm is based on a comparison between the co- and cross-polarized coherence of clutter and that of a power line. In practice, the coherence is estimated from the average of a finite number of the measured samples (pixels) of the random variable. Hence, the estimate itself is a random variable which, in most cases, has the same mean as the original random variable with a much smaller variance. In this particular case where the normalized correlation coefficient is always a positive quantity, the ensemble average of the coherence estimate is always larger than the coherence ($\langle\hat{\gamma}\rangle > \gamma$). For example the clutter coherence is zero and the mean coherence estimate is

a positive quantity. In order to quantify the false-alarm rate and the probability of detection (PD), probability density functions (pdfs) of clutter coherence and coherence of pixels including power line segments are needed.

Assuming the clutter statistics is described by a Gaussian process, the pdf of the estimate of co- and cross-polarized coherence can be derived analytically. Suppose N pixels are used to estimate the coherence, then the pdf of ($\hat{\gamma}$) is given by [14]

$$p(\hat{\gamma}) = 2(N-1)(1-\gamma^2)^N \hat{\gamma}(1-\hat{\gamma}^2)^{N-2} F(N, N; 1; \gamma^2\hat{\gamma}^2) \tag{2}$$

where γ is the coherence and F is the hypergeometric function also known as the Gauss' hypergeometric function [12]. For clutter where $\gamma = 0$, the pdf given by (2) simplifies significantly and is given by

$$p(\hat{\gamma}) = 2(N-1)\hat{\gamma}(1-\hat{\gamma}^2)^{N-2}. \tag{3}$$

For pixels including power line segments, the coherence is a function of power-line backscatter as well as clutter backscattering coefficients. Adding the clutter backscatter of a pixel ($\sigma^o A$) to that of the power-line incoherently, it can easily be shown that the coherence of pixels including power line segments is given by

$$\gamma = \frac{|\sigma^p_{vv,hv}|}{\sqrt{(\sigma^\circ_{vv}A + \sigma^p_{vv})(\sigma^\circ_{hv}A + \sigma^p_{hv})}} \tag{4}$$

where $\sigma^p_{vv,hv} = 4\pi S_{vv}S^*_{hv}$, σ^p_{vv}, and σ^p_{hv} are, respectively, the cross correlation between VV and HV backscatter, and VV and HV radar cross section of the power-line segment in each pixel. Also, σ°_{vv} and σ°_{hv} are the clutter backscattering coefficients and A is the pixel area. Substitution of (4) in (2) provides the pdf for the estimate of coherence for pixels that include the power line. Using the measured polarimetric backscatter data from the power line whose RCS is shown in Fig. 3, the coherence of the power line 3 in different clutter backgrounds is shown in Fig. 4. Here it is assumed that the radar pixel is 30 cm $\times$ 30 cm and the clutter cross- to co-polarized ratio $\sigma^\circ_{hv}/\sigma^\circ_{vv} = -10$ dB. It should be pointed out here that since the increase in the power-line RCS with decreasing the resolution is slower than the increase in pixel area, radars with finer resolutions provide higher coherence for pixels that include power lines.

Successful detection and false-alarm rate depend on the separation between the mean values of clutter and power-line coherence estimate and on the narrowness of their density functions. Fortunately, closed-form solutions for the moments of coherence estimate exist. The first and second moments are given by

$$\langle\hat{\gamma}\rangle = \frac{\Gamma(N)\Gamma(3/2)}{\Gamma(N+1/2)}\,{}_3F_2(3/2, N, N; N+1/2, 1; \gamma^2) \cdot (1-\gamma^2)^N$$

$$\langle\hat{\gamma}^2\rangle = \frac{1}{N}\,{}_3F_2(2, N, N; N+1, 1; \gamma^2)(1-\gamma^2)^N$$

where ${}_pF_q$ is the generalized hypergeometric series and Γ is the gamma function. Noting that ${}_3F_2(2, N, N; N+1, 1; 0) = 1$, the mean and the second moment of the coherence estimate of the clutter simplify to

$$\langle\hat{\gamma}\rangle = \frac{0.8862\Gamma(N)}{\Gamma(N+1/2)}, \qquad \langle\hat{\gamma}^2\rangle = \frac{1}{N}$$

which are only a function of number of independent samples. Using the large argument expansion of gamma function (Stirling formula), the mean of the coherence estimate for large $N > 10$ may be evaluated from

$$\langle\hat{\gamma}\rangle = \frac{0.8862}{\sqrt{N}}.$$

In this case, the standard variation is simply equal to $0.463/\sqrt{N}$.

To demonstrate the procedure for the calculation of the false-alarm rate and the probability of detection let us assume that $N = 300$ pixels are available for estimating the coherence and the coherence of pixels with power line is $\gamma = 0.2$. Fig. 5 shows the pdfs of the clutter and power line for this example. Also shown in this figure is a threshold (γ_T) above which power-line detection is flagged. The percentage of the time (probability) that the clutter coherence exceed the threshold level is the false-alarm rate and the probability that power-line coherence is above the threshold level is the probability of detection. There is a tradeoff between the false-alarm rate and

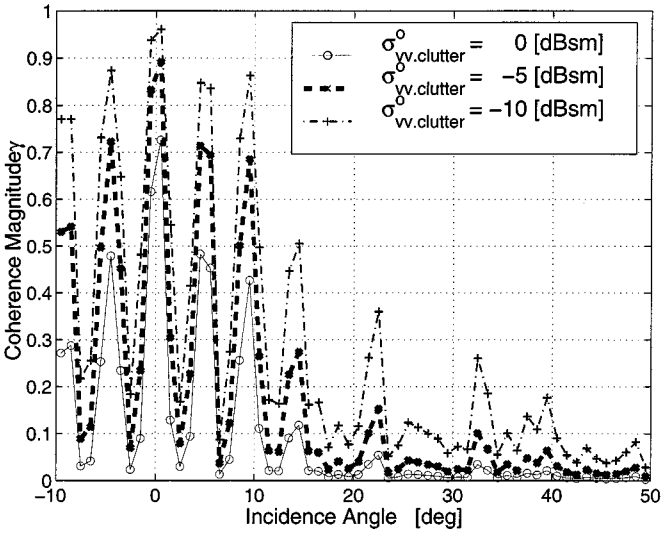

Fig. 4. Coherence of the power line shown in Fig. 3 in different background clutter with $\sigma^0_{hv}/\sigma^0_{vv} = -10$ dB.

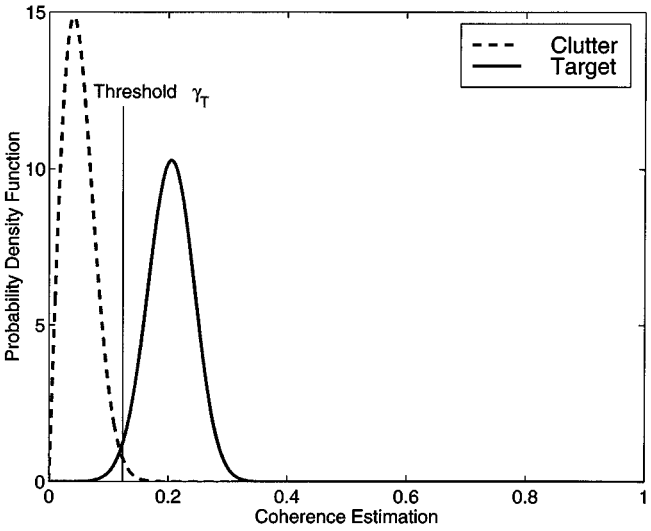

Fig. 5. Probability density function of clutter ($\gamma = 0$) and power line in clutter ($\gamma = 0.2$) using $N = 300$ independent samples. A threshold level is also shown. The areas under curves beyond γ_T are the FAR and PD.

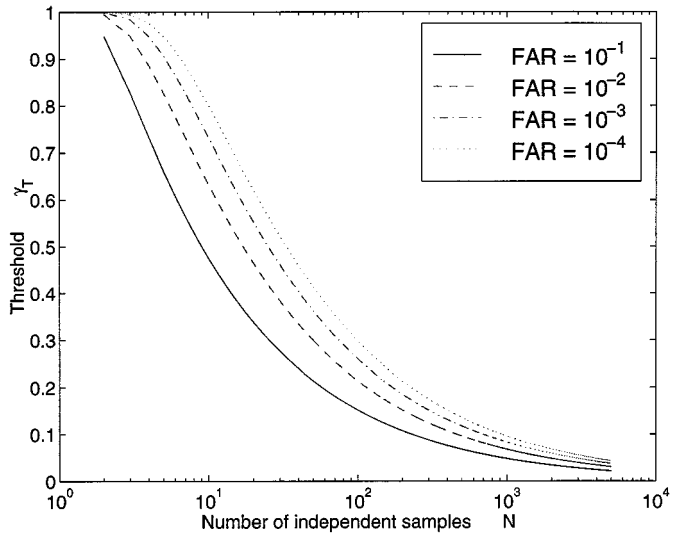

Fig. 6. Threshold level as a function of number of independent samples for different values of FAR.

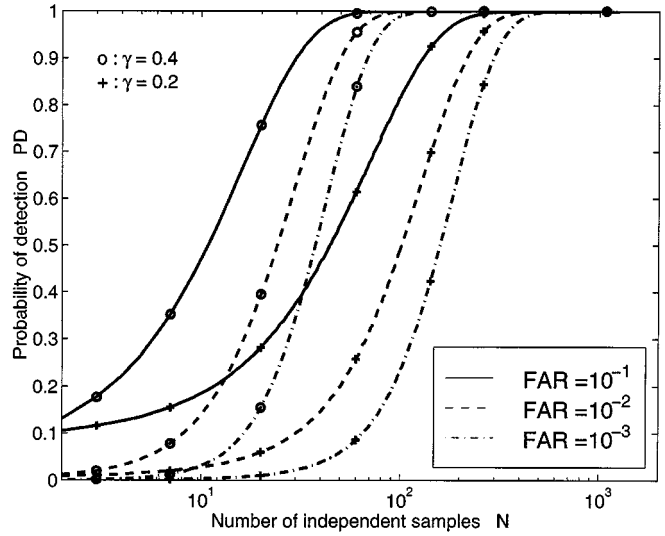

Fig. 7. Probability of detection as a function of number of independent samples and for different values of FAR and coherence values of power lines in clutter.

the probability of detection. The lower is the false-alarm rate the lower would be the probability of detection. The false-alarm rate (FAR) can explicitly be related to the threshold level and the number of independent samples using (3)

$$\text{FAR} = 2(N-1)\int_{\gamma_T}^{1} \hat{\gamma}(1-\hat{\gamma}^2)^{N-2} d\hat{\gamma},$$

which renders the following relationship:

$$\gamma_T = \sqrt{1 - \text{FAR}^{(1/N-1)}}.$$

In a similar manner the probability of detection (PD) can be computed from (2)

$$\text{PD} = 1 - 2(N-1)(1-\gamma^2)^N \int_0^{\gamma_T} \cdot \hat{\gamma}(1-\hat{\gamma}^2)^{N-2} F(N, N; 1; \gamma^2\hat{\gamma}^2) d\hat{\gamma}. \quad (5)$$

Unfortunately, a simple closed form for (5) cannot be obtained; however, using the series expansion representation of the hypergeometric function the probability of detection in terms of a chosen FAR and number of independent samples can be obtained from

$$\text{PD} = 1 - (N-1)(1-\gamma^2)^N \sum_{k=0}^{\infty}\sum_{j=0}^{N-2} \left(\frac{(N+k-1)!\gamma^k}{(N-1)!k!}\right)^2 \cdot \frac{(N-2)!}{(N-j-2)!j!(j+k+1)} \left(1-\text{FAR}^{(1/(N-1))}\right)^{(j+k+1)}.$$

Usually γ_T is a relatively small number (<0.2) and only few terms in k are sufficient for calculating PD. Fig. 6 shows the threshold level as a function of number of independent samples for different values of FAR. Also, Fig. 7 shows the PD as a function of number of independent samples and different values of FAR and γ.

V. Performance of Detection Algorithm

The performance of the polarimetric detection algorithm at W-band frequencies was demonstrated under laboratory conditions earlier [6]. In this section, the performance of the algo-

TABLE I
DETECTION PERFORMANCE

	$\langle\|S_{vv}\|^2\rangle$	$\langle\|S_{hv}\|^2\rangle$	$\frac{\langle S_{vv}S_{hv}^*\rangle}{\sqrt{\langle\|S_{vv}\|^2\rangle\langle\|S_{hv}\|^2\rangle}}$	$\frac{\langle S_{hh}S_{hv}^*\rangle}{\sqrt{\langle\|S_{vv}\|^2\rangle\langle\|S_{hv}\|^2\rangle}}$	SUM
Power line 1(image 1)	3.80e-2	2.73e-3	6.13e-2	4.74e-2	1.08e-1
Power line 2(image 1)	2.69e-2	1.68e-3	8.43e-2	4.18e-2	1.02e-1
Power line 3(image 1)	4.05e-2	2.91e-3	6.26e-2	3.96e-2	1.19e-1
Clutter 1(image 1)	4.14e-2	2.29e-3	2.01e-2	1.18e-2	2.59e-2
Clutter 2(image 1)	3.98e-2	2.59e-3	1.12e-2	2.48e-2	1.78e-2
Clutter 3(image 1)	2.77e-2	1.81e-3	4.07e-2	3.11e-2	6.96e-2
Power line 1(image 2)	4.23e-2	3.14e-3	6.62e-2	5.80e-2	1.22e-1
Power line 2(image 2)	3.84e-2	3.19e-3	7.54e-2	6.44e-2	1.38e-1
Power line 3(image 2)	4.37e-2	3.16e-3	8.07e-2	6.08e-2	1.38e-1
Clutter 1(image 2)	2.39e-2	1.74e-3	6.22e-3	2.02e-2	2.58e-2
Clutter 2(image 2)	4.08e-2	2.60e-3	1.07e-2	4.36e-2	4.15e-2
Clutter 3(image 2)	1.56e-2	1.21e-3	2.93e-2	3.75e-2	6.55e-2
Power line 1(image 3)	3.07e-02	2.62e-0	2.45e-01	3.11e-01	5.50e-01
Power line 2(image 3)	2.47e-02	2.58e-03	1.73e-01	1.76e-01	3.39e-01
Power line 3(image 3)	2.65e-02	2.68e-03	1.86e-01	2.68e-01	4.30e-01
Clutter 1(image 3)	1.75e-02	2.08e-03	6.19e-02	2.65e-02	6.35e-02
Clutter 2(image 3)	1.87e-02	1.89e-03	2.74e-02	1.23e-02	3.65e-02
Clutter 3(image 3)	1.86e-0	2.03e-03	6.57e-02	4.46e-02	2.13e-02
Power line 1(image 4)	4.31e-02	2.65e-03	4.19e-01	4.17e-01	8.16e-01
Power line 2(image 4)	1.88e-02	2.07e-03	1.89e-01	2.16e-01	4.04e-01
Power line 3(image 4)	3.89e-02	2.78e-03	4.30e-01	4.73e-01	8.82e-01
Clutter 1(image 4)	9.97e-03	1.71e-03	7.62e-02	6.40e-02	1.09e-01
Clutter 2(image 4)	9.04e-03	1.63e-03	5.17e-02	2.95e-02	5.83e-02
Clutter 3(image 4)	1.03e-02	1.69e-03	4.63e-02	5.03e-02	8.70e-02
Power line 1(image 5)	4.23e-02	3.25e-03	1.67e-01	1.54e-01	3.06e-01
Power line 2(image 5)	2.84e-02	2.73e-03	5.33e-02	4.99e-02	1.02e-01
Power line 3(image 5)	4.87e-02	2.98e-03	2.27e-01	2.39e-01	4.51e-01
Clutter 1(image 5)	2.82e-02	2.32e-03	3.75e-02	1.81e-02	4.71e-02
Clutter 2(image 5)	2.86e-02	2.58e-03	3.62e-02	5.56e-02	6.21e-02
Clutter 3(image 5)	2.03e-02	2.05e-03	4.18e-02	4.58e-02	5.48e-02
Power line 1(image 6)	2.47e-02	2.46e-03	9.48e-02	7.23e-02	1.53e-01
Power line 2(image 6)	1.40e-02	1.76e-03	1.31e-01	1.09e-01	2.24e-01
Power line 3(image 6)	1.92e-02	2.06e-03	1.06e-01	5.02e-02	1.42e-01
Clutter 1(image 6)	1.10e-02	1.90e-03	3.70e-02	4.20e-02	1.44e-02
Clutter 2(image 6)	1.25e-02	1.83e-03	4.49e-02	8.46e-02	4.03e-02
Clutter 3(image 6)	1.05e-02	1.53e-03	7.77e-02	7.43e-02	2.17e-02
Power line 1(image 7)	8.50e-3	2.14e-3	4.72e-2	7.99e-2	1.23e-1
Power line 2(image 7)	9.59e-3	2.15e-3	8.17e-2	9.23e-2	1.73e-1
Power line 3(image 7)	1.24e-2	2.38e-3	1.76e-1	8.11e-2	2.57e-1
Clutter 1(image 7)	7.53e-3	1.89e-3	1.70e-2	2.62e-2	1.54e-2
Clutter 2(image 7)	7.53e-3	1.88e-3	3.12e-2	3.78e-2	6.83e-2
Clutter 3(image 7)	7.08e-3	1.87e-3	2.78e-2	1.65e-2	3.49e-2

rithm is examined using polarimetric data acquired by a millimeter-wave synthetic aperture radar. As discussed in the previous section the FAR and the PD are functions of the number of available independent samples and the coherence of pixels that include the power line. Referring to Fig. 5, it is obvious that the coherence of the pixels with power lines is a function of clutter backscattering coefficients, power-line aspect angle, and the power-line RCS. RCS of power lines increases with increasing frequency especially at aspect angles beyond 15° for normal (see typical RCS values at Ka-band and W-band reported in [5] and [6]). However, the backscattering of clutter at millimeter-wave frequency is not a strong function of frequency. Therefore, the higher the radar frequency, the higher will be the coherence of pixels with power lines.

The only polarimetric millimeter-wave SAR data available are those acquired by the Lincoln Laboratory Ka-band polarimetric SAR [15]. This radar operates at the center frequency of 35 GHz and has a bandwidth of 500 MHz. The radar-antenna beamwidth is 2° and can provide radar images with resolution of 30 cm × 30 cm. In order to investigate the behavior of radar clutter at low grazing incidence, the Lincoln Lab Ka-band SAR was flown at low altitudes and a large number of polarimetric SAR images were acquired. Among these seven images, which included power lines, were identified and selected for the performance assessment of the algorithm. High-resolution aerial photograph of radar scenes are also available. Using the aerial photographs, the radar images were chosen so that they contained a wide range of clutter types and power-line aspect angles.

Suspended power lines between two towers conform to a catenary whose sag in the middle is a function of tower separation, tensile strength, temperature, and ice loading. This sag can be as high as 6 m. For high-incidence angels, depending on the radar range resolution, power lines are mapped as a straight lines between the two towers. For example, a power line with

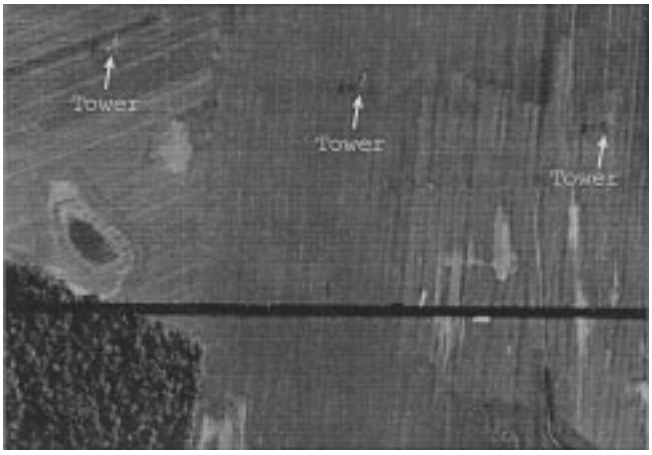

Fig. 8. An aerial photograph of a test site.

6 m sag in the middle is within one range resolution of 30 cm for incidence angles higher than 85°. Using the photo images, the location of towers and power lines were identified in the radar scenes. The scattering matrices of 21 linear regions, 2 pixel wide and almost 1000 pixel long ($N \approx 2000$), in the seven radar images along the power line segments were extracted. Also similar scattering matrices were extracted from clutter regions within each image. The results are summarized in Table I where the backscatter power in VV and HV channels together with VV-HV and HH-HV coherences and their sum for both power line and clutter regions are reported. In all cases examined, backscattering coefficient of clutter $\sigma^0_{vv} < -10$ dB and the ratio of cross- to co-polarized backscatter $\sigma^0_{hv}/\sigma^0_{vv} < -10$ dB. Use of any single or combined backscatter power does not result in an effective detection. On the other hand the proposed detection algorithm based on co- to cross-polarized backscatter coherence clearly identifies the power lines in all 21 regions. In these examples, the signal-to-clutter ratio ranges from 2 to 10, depending on the power lines and their background clutter. As expected, signal-to-clutter ratio for power lines illuminated at low aspect angles is higher than those illuminated at high-aspect angles. Figs. 8 and 9 show a typical aerial photograph and the corresponding SAR image that includes a power line. Power lines are not visible, however, the tower supporting the power line are somewhat discernible. Fig. 10 shows the same SAR image after the detection process where the location of power lines are indicated.

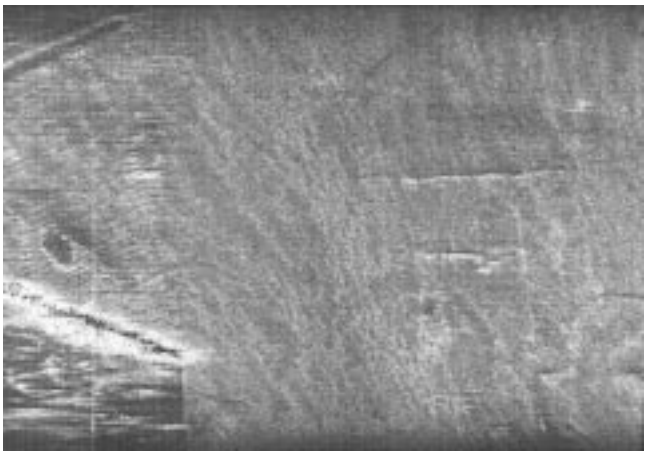

Fig. 9. An example of SAR image including a power line section before detection.

Fig. 10. The SAR image shown in Fig. 9 after detection of power lines.

VI. Conclusion

Problem of power line detection in polarimetric SAR images was considered in this paper. Performance of a statistical polarimetric detection algorithm was evaluated using seven polarimetric SAR scenes at Ka-band. Analytical formulations for the calculation of FAR and probability of detection in terms of number of independent samples and the coherence of pixels which include power line were obtained. It was shown that the PD and FAR are both improved by increasing the frequency and decreasing the resolution of the SAR system. It was also shown that the power-line coherence decreases at higher aspect angles (angle between flight path and power line direction), which results in lower PD. In the examples considered here, the detection algorithm successfully identified all 21 power-line segments in the SAR images.

Acknowledgment

The authors appreciate the help of J. Costanza of the Army Research Laboratory for providing the Lincoln Laboratory SAR images.

REFERENCES

[1] B. Rembold, H. G. Wippich, M. Bischoff, and W. F. X. Frank, "A MM-wave collision warning sensor for helicopters," *Proc. Military Microwave*, pp. 344–351, 1982.

[2] H. H. Al-Khatib, "Laser and millimeter-wave backscatter of transmission cables," *SPIE vol. 300 Phys. Technol. Coherent Infrared Radar*, pp. 212–229, 1981.

[3] M. Savan and D. N. Barr, "Reflectance of wires and cables at 10.6 micrometer," Center for Night Vision and Electro-Optics, MSEL-NV-TR-0063, Jan. 1988.

[4] K. Sarabandi and M. Park, "A radar cross section model for power lines at millimeter-wave frequencies," *IEEE Trans. Antennas Propagat.*, Jan. 1999.

[5] K. Sarabandi, L. Pierce, Y. Oh, and F. T. Ulaby, "Power lines: Radar measurements and detection algorithm for polarimetric SAR images," *IEEE Trans. Aerosp. Electron. Syst.*, vol. 30, pp. 632–648, Apr. 1994.

[6] K. Sarabandi and M. Park, "Millimeter-wave radar phenomenology of power lines and a polarimetric detection algorithm," *IEEE Trans. Antennas Propagat.*, Sept. 1998.

[7] F. T. Ulaby and C. Elachi, *Radar Polarimetry for Geoscience Applications*. Dedham, MA: Artech House, 1990.

[8] A. Nashashibi, F. T. Ulaby, and K. Sarabandi, "Measurement and modeling the millimeter-wave backscatter response of soil surfaces," *IEEE Trans. Antennas Propagat.*, vol. 34, pp. 561–572, Mar. 1996.

[9] K. Sarabandi, E. S. Li, and A. Nashashibi, "Modeling and measurements of scattering from road surfaces at millimeter-wave frequencies," *IEEE Trans. Antennas Propagat.*, vol. 45, pp. 1679–1688, Nov. 1997.

[10] E. S. Li and K. Sarabandi, "Low grazing incidence millimeter-wave scattering models and measurements for various road surfaces," *IEEE Trans. Antennas Propagat.*, vol. 47, May 1999.

[11] J. B. Mead, A. L. Pazmany, P. S. Chang, and R. E. McIntosh, "Comparison of coherent and noncoherent polarimetric radar measurement at 95 GHz," *Radio Sci.*, vol. 31, no. 2, pp. 325–333.

[12] L. S. Gradshteyn and I. M. Ryzhik, *Table of Integrals, Series, and Products*. San Diego, CA: Academic, 1980.

[13] F. T. Ulaby, A. Nashashibi, A. El-Rouby, E. Li, R. Deroo, K. Sarabandi, R. Wellman, and B. Wallace, "95-GHz scattering by terrain at near-grazing incidence," *IEEE Trans. Antennas Propagat.*, vol. 46, pp. 3–13, Jan. 1998.

[14] R. Touzi and A. Lopes, "Statistics of the Stokes parameters and of the complex coherence parameters in one-look and multi-look speckle field," *IEEE Trans. Geosci. Remote Sensing*, vol. 34, pp. 519–532, Mar. 1996.

[15] J. C. Henry, "The Lincoln Laboratory 35 GHz airborne polarimetric SAR imaging radar system," in *IEEE Nat. Telesyst. Conf.*, Atlanta, GA, Mar. 1991.

Kamal Sarabandi (S'87–M'90–SM'92–F'00) received the B.S. degree in electrical engineering from Sharif University of Technology, Tehran, Iran, in 1980, the M.S.E. degree in electrical engineering in 1986, and the M.S. (mathematics) and Ph.D. (electrical engineering) degrees in 1989, all from the University of Michigan, Ann Arbor.

From 1980 to 1984, he worked as a Microwave Engineer in the Telecommunication Research Center. He is presently the Director of the Radiation Laboratory, Department of Electrical Engineering and Computer Science, University of Michigan. He has 18 years of experience with microwave sensors and radar systems. In the past eight years, he has served as the Principal Investigator and Co-Investigator on many projects sponsored by NASA, JPL, ARO, ONR, ARL, NSF, and numerous industries. He has published many book chapters and more than 85 papers in refereed journals on electromagnetic scattering, random media modeling, wave propagation, microwave measuring techniques, radar calibration, application of neural networks in inverse scattering problems, and microwave sensors. He has also had more than 150 papers and invited presentations in national and international conferences and symposia on similar subjects.

Dr. Sarabandi is listed in *American Men & Women of Science* and *Who's Who in Electromagnetics*. He is a member of the IEEE Geoscience and Remote Sensing ADCOM since January of 1998 and served as the Chairman of Geoscience and Remote Sensing Society Southeastern Michigan chapter from 1992–1998. He is also a member of Commission F of URSI and of The Electromagnetic Academy. He was a recipient of a 1996 Teaching Excellence Award, the 1997 Henry Russel Award from the Regent of The University of Michigan, and the 1999 GAAC Distinguished Lecturer Award from the German Federal Ministry for Education, Science, and Technology.

Moonsoo Park was born in Seoul, South Korea, on February 4, 1964. He received the B.S. and M.S. degrees in electronics engineering from Seoul National University, Seoul, South Korea, in 1987 and 1989, respectively. He is currently working toward the Ph.D. degree in electrical engineering at the University of Michigan, Ann Arbor.

From 1989 to 1993, he worked as an RF/Microwave Design Engineer in Daewoo Electronics, Seoul, South Korea. He is currently a Research Assistant with the Radiation Laboratory, the University of Michigan, Ann Arbor. His research interests include polarimetric millimeter-wave radar systems for navigations, millimeter-wave remote sensing, wave scattering, and SAR image processing.